Numerical Error Estimation in Particle Tracking Measurement behind a Shock Wave

by

Youhei Shinohara, Kazuyuki Toda[(1)] and Makoto Yamamoto[(2)]

Tokyo University of Science

Department of Mechanical Engineering

1-3, Kagurazaka, Shinjuku-ku, Tokyo, 162-8601, Japan

[(1)]E-Mail: ktoda@rs.kagu.tus.ac.jp

[(2)]E-Mail: yamamoto@rs.kagu.tus.ac.jp

ABSTRACT

Measuring techniques such as Laser Doppler Velocimetry (LDV), Particle Image Velocimetry (PIV), Particle Tracking Velocimetry (PTV), Holographic Particle Image Velocimetry (HPIV) and so on depend on the velocity information obtained from a micron-sized particle travelling in a fluid. The traceability of these particles to any velocity changes in a flow field is one of the key assumptions, in applying such techniques successfully. However, in the flow field with large velocity gradient, this assumption would become improper. That is, the relative velocity between fluid and particle becomes large, and thus the measuring error cannot be accepted.

This paper shows a numerical investigation for the motion of tracer particles in the presence of steep velocity gradient across a steady and an oscillating shock wave. Various particles with different radius and density are taken into account. The particle motions are simulated, by using Basset-Boussinesq-Oseen (BBO) equation. The distributions of physical quantities within a shock wave are obtained through the weak shock theory.

First, the contribution of each term in the BBO equation to particle behaviour is numerically investigated for a steady shock wave case. Nine kinds of particles are tested. The results indicate that, (1) for the small density particle, the drag force is dominant, but the pressure gradient and the Basset terms should be considered, (2) the non-dimensional settling length can be estimated only from the particle diameter.

Second, the effects of shock wave oscillation and nonuniform particle size are investigated, to realize the more exact experimental conditions. The numerical results suggest that (3) the turbulence detected in measurements contains the considerably large amount of errors concerning with the particle property used as the seeding particle, (4) especially, the effect of the dispersion of particle diameter is more serious.

1. INTRODUCTION

Measuring techniques such as Laser Doppler Velocimetry (LDV), Particle Image Velocimetry (PIV), Particle Tracking Velocimetry (PTV), Holographic Particle Image Velocimetry (HPIV) and so on depend on the velocity information obtained from a micron-sized particle travelling in a fluid. The traceability of these particles to any velocity changes in a flow field is one of the key assumptions, in applying such techniques successfully. However, in the flow field with large velocity gradient, this assumption would become improper. That is, the relative velocity between fluid and particle becomes large, and thus the measuring error cannot be accepted. Although a number of researchers have investigated this gas/particle two-phase flow phenomenon analytically, experimentally and/or numerically, the detail of the phenomenon has not been clarified, and thus the method to correct the particle velocity measured with LDV, PTV and so on has not been established yet (Tedeshi et al.,1999, Thomas,1992, Maurice,1992). Furthermore, the erroneous profiles of mean and turbulent quantities behind a shock wave prevent designers and modellers from developing better machines and constructing a improved compressible turbulence model.

This paper shows a numerical investigation for the motion of tracer particles in the presence of steep velocity gradient across a steady and an oscillating shock wave. Various particles with different radius and density are taken into account. The particle motions are simulated, by using Basset-Boussinesq-Oseen (BBO) equation. The distributions of physical quantities within a shock wave are obtained through the weak shock theory.

First, the contribution of each term in the BBO equation to particle behaviour is numerically investigated for a steady shock wave case. Nine kinds of particles are tested. The density is varied from 10 to 1000[kg/m^3], and the diameter from 1 to 100[m m]. The results indicate that, (1) for the small density particle, the drag force is dominant, but the pressure and the Basset terms should be considered, (2) the non-dimensional settling length can be estimated only from the particle diameter.

Second, the effects of shock wave oscillation and non-uniform particle size are studied, to realize the more exact experimental conditions. The shock frequency was varied from 0 to 100[kHz]. The numerical results suggest that (3) the turbulence detected in measurement contains the considerably large amount of errors concerning with the particle property used as the seeding particle, (4) especially, the dispersion of particle diameter is more serious.

2. NUMERICAL PROCEDURES

2.1 Particle Motion

The flow field is compressible and gas/solid two-phase flow. First, we assumed that the concentration of particles is small, and the collision among particles can be neglected (i.e. one-way coupling). A various kinds of forces act on particles in a fluid. Although many researchers have proposed the governing equation, following the work by Mei (1996), Basset-Boussinesq-Oseen (BBO) equation expressed as follows is the most suitable,

$$m_p \frac{dv_i}{dt} = (m_p - m_f) g_i + m_f \frac{Du_i}{Dt} - \frac{1}{2} m_f \left(\frac{dv_i}{dt} - \frac{Du_i}{Dt} - \frac{1}{10} a^2 \frac{\partial^2 u_i}{\partial x_j^2} \right)$$
$$- 6\pi a \mu f \left(v_i - u_i - \frac{1}{6} a^2 \frac{\partial^2 u_i}{\partial x_j^2} \right) - 6\pi a^2 \mu \int_0^t dt \left(\frac{\frac{d}{dt}\left(v_i - u_i - \frac{1}{6} a^2 \frac{\partial^2 u_i}{\partial x_j^2} \right)}{(\pi \nu (t-t))^{1/2}} \right) + F_{etc} \quad (1)$$

where m means the mass, v_i is the velocity of a particle, u_i the velocity of fluid, a the radius of a particle, μ the viscosity of fluid, ν the kinematic viscosity, f the drag coefficient, g_i the gravitational acceleration, and subscripts p and f denote particle and fluid, respectively. Each term in the right-hand side of Eq.(1) means the body force such as gravitation and buoyancy, the force by the pressure gradient, the additional mass force, the drag force, the Basset history force, and another forces such as Saffman and temperature gradient forces. In the present study, the first and last terms were neglected because of the flow conditions described later.

The relation between a particle position and its velocity can be given by

$$\frac{dx_{pi}}{dt} = v_i \quad (2)$$

where x_{pi} is the particle position. Assuming a particle is sphere, the masses of a particle and fluid are expressed by

$$m_p = \frac{4}{3}\pi a^3 \rho_p \quad , \quad m_f = \frac{4}{3}\pi a^3 \rho_f \tag{3}$$

where ρ denotes density. The drag coefficient f can be provided with the relative Reynolds number as

$$\phi = 1 + 0.15\,Re_p^{0.687} \quad , \quad \mathrm{Re}_p = \frac{2a|u_i - v_i|}{\nu} \tag{4}$$

In all the computations, we adopted 4-stage Runge-Kutta method to assure the accuracy for time integration.

2.2 Flow Field

In the present study, we focused on the very small particles whose thickness is nearly same as a shock wave thickness. The distributions of physical quantities within a shock wave play important roles on the particle motions. Therefore, we provided the exact distributions within a shock wave, using the weak shock-wave theory.

Assuming x is the normal direction to a shock wave, and u is the velocity component, we can obtain

$$\frac{u_1}{u_1 - u_2}\ln\left(\frac{2(u_1 - u)}{u_1 - u_2}\right) - \frac{u_1}{u_1 - u_2}\ln\left(\frac{2(u - u_2)}{u_1 - u_2}\right) = \frac{8}{3}\frac{\rho_{f1} u_1}{\mu}\frac{\gamma - 1}{\gamma}x \tag{5}$$

where subscripts *1* and *2* mean the upstream and downstream value of a shock, respectively, and γ denotes the specific heat.

The thickness of a shock wave based on the maximum velocity gradient can be expressed as

$$X_u = \frac{u_1 - u_2}{\left|\frac{du}{dx}\right|_{\max}} = \frac{8}{G}\frac{\mu_1}{(u_1 - u_2)\rho_{f1}} \quad , \quad G = \frac{\gamma + 1}{\frac{4}{3} + \frac{\gamma - 1}{\mathrm{Pr}}} \tag{6}$$

where Pr is the Prandtl number.

In the present study, the velocity distribution was determined, solving Eq.(5). The density and the static temperature of fluid were computed by using the computed velocity by Eq.(5), continuity equation, momentum equation and state equation of perfect gas. The viscosity was given with Sutherland's formula.

2.3 Computational Conditions

We have studied three cases. The first is the case with a steady shock and a single particle, the second is that with an oscillating shock wave (i.e. unsteady case) and a single particle, and the last is that with a unsteady shock and multiple particles. The detail of these computational conditions will be explained below.

(1) Steady shock and single particle case
As the ideal state, we calculated the cases where a shock wave is steady. The upstream conditions of fluid are listed in Table 1, and the computed velocity distribution is shown in Fig.1. These conditions were common in all computations. And, as shown in Table 2, we employed nine kinds of particle characteristics in terms of the particle diameter and the density.

Table 1 Upstream Conditions of Fluid

Mach Number	M_1		1.1
Density	ρ_{f1}	[kg/m^3]	1.2
Static Temperature	T_1	[K]	293.2

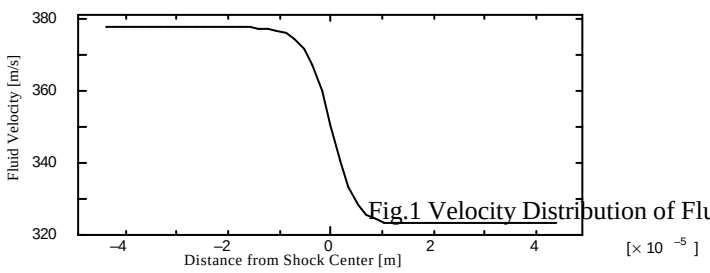

Fig.1 Velocity Distribution of Fluid Flow

Table 2 Particle Conditions in Steady Shock Case

Particle Diameter• Density	1.0• 10[1] [kg/m³]	1.0• 10[2] [kg/m³]	1.0• 10[3] [kg/m³]
1.0 [μm]	CaseA1	CaseA2	CaseA3
10.0 [μm]	CaseB1	CaseB2	CaseB3
100.0[μm]	CaseC1	CaseC2	CaseC3

(2) Unsteady shock and single particle case

Generally, a shock wave is oscillating with relatively high frequency (Dolling and Bogdonoff,1981, Dolling and Or,1983, Coe et al.,1973). As the second state, we calculated the cases where a shock wave is oscillating. The flow and the particle conditions were same as those of the steady case, shown in Tables 1 and 2. The oscillating frequencies were set 1, 10 and 100[kHz], and the amplitude was 5[mm]. These conditions were determined, based on the experiment carried out by Dolling and Or (1983) for the compression ramp and the bunt leading edge airfoil. The phase angle was defined to be 0[deg.], when a particle enters the shock region at the most upstream of the oscillation.

(3) Unsteady shock and multiple particle case

Finally, the size distribution of particles was considered. We adopted five kinds of tracer particles that are generally used in LDV measurement in Japan; MB-S, MX-150, MX-300, MX-500 and MX-1000. The particle material is acrylic. The particle characteristics are listed in Table 3, and the histogram of size distributions are exhibited in Fig.2. MX-150 has the smallest mean diameter, and MX-1000 does the maximum. On the other hand, MX-150 has the broadest dispersion, and MX-1000 does the narrowest one. Others are in between. In the computations, the profile of size distribution was divided into 100 kinds of particle diameters as seen in Fig.2.

Table 3 Conditions of Tracer Particles

Tracer	Mean Diameter [μm]	Range of Diameter [μm]	Density [kg/m³]
MB-S	5.71	0.5-13.1	1.19• 10[3]
MX-150	2.70	0.5-15.6	1.19• 10[3]
MX-300	3.29	0.7-16.6	1.19• 10[3]
MX-500	5.58	2.3-9.3	1.19• 10[3]
MX-1000	9.69	0.5-13.1	1.19• 10[3]

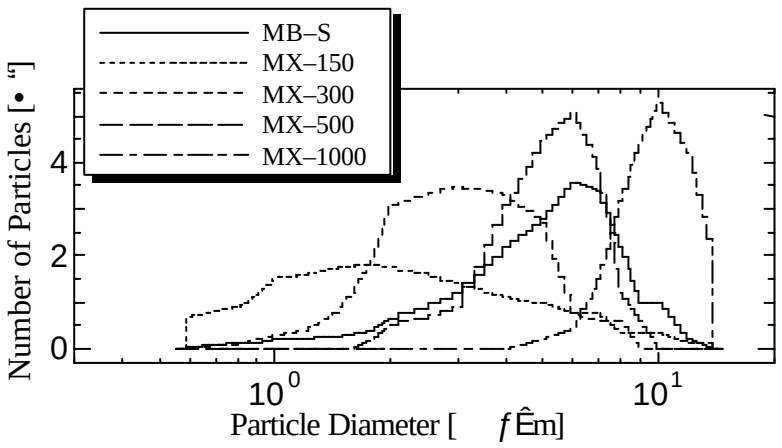

Fig.2 Histogram of Tracer Particles

The settling length is important to estimate the measuring error, or determine the region where error is relatively large. In the present study, it was defined as the distance between a shock centre and the position where a relative velocity of particle becomes less than 5.0[m/s]. The difference 5.0(m/s) corresponds to about 1.3% of the upstream velocity of fluid.

3. NUMERICAL RESULTS AND DISCUSSION

3.1 Steady Shock and Single Particle Case

The contributions of each term in the BBO equation across the shock wave are summarized in Fig.3. First, it is confirmed that the contributions by the pressure gradient and the Basset terms become important, when the particle density and diameter are small. Second, when the particle density is constant, the pressure gradient and the additional mass terms decrease with increasing the particle density. Third, the drag and the Basset terms do not rapidly decrease with increasing the particle density. This is why the relative velocity is large and the traceability becomes worse. Forth, when the particle density is constant, the Basset and the drag terms become relatively smaller, and thus the pressure gradient and additional mass terms are larger. However, the acceleration by these two terms is limited near the shock and the global effect by these two terms is small.

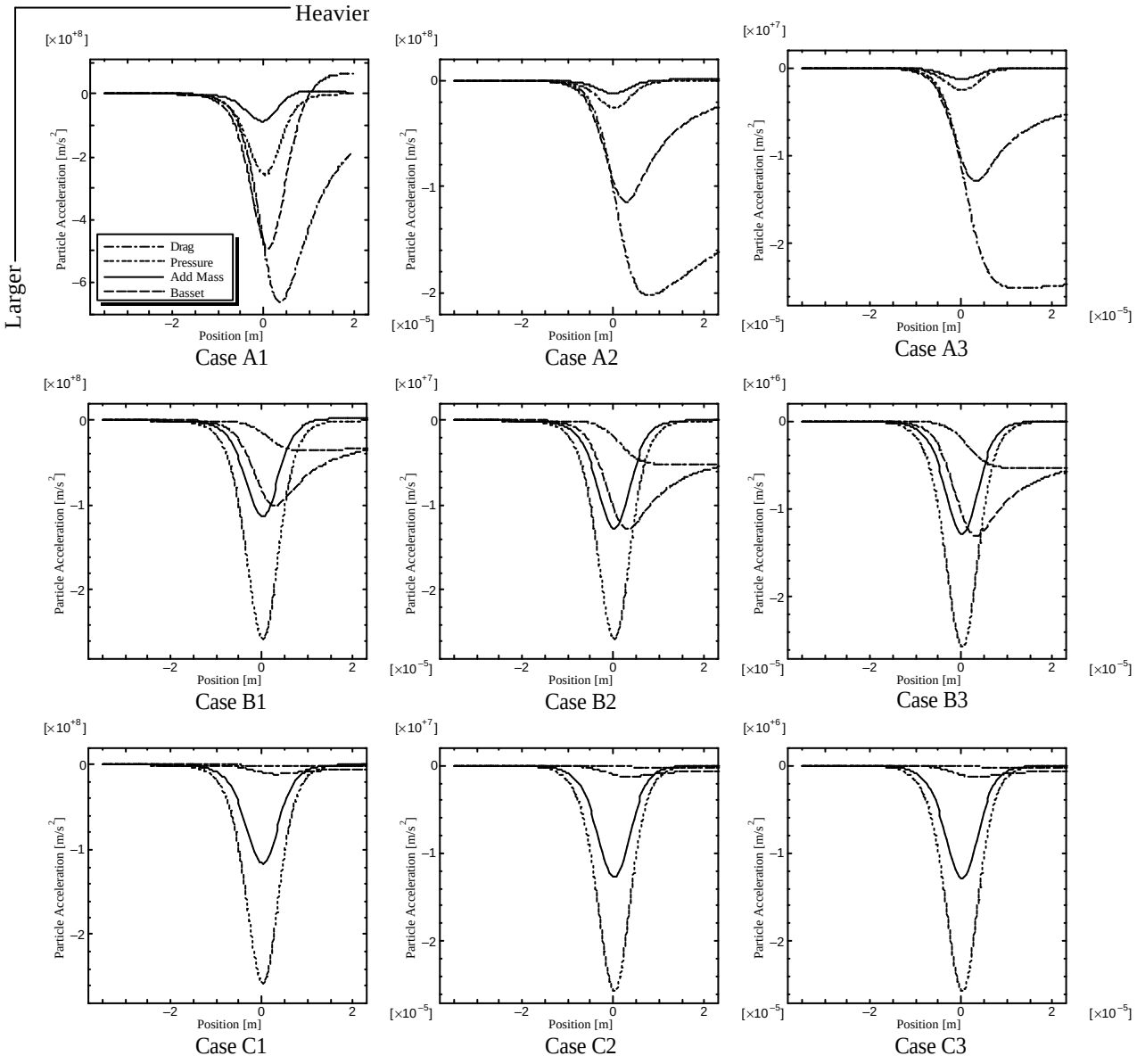

Fig.3 Contribution of Each Term in BBO Equation across Shock Wave

The settling lengths of different particles are exhibited in Figs.4 and 5. The non-linear increase of the settling length for the particle radius and the linear increase for the particle density are clearly seen. These trends are similar to the early work performed by Maxwell and Seasholtz (1974) for the upstream Mach number of 1.6.

It would be important and helpful to derive the non-dimensional settling length, in order to estimate the measuring error. Assuming the acting force is only drag, and integrating BBO equation, we can obtain the next relation.

$$\frac{x}{\tau_p u_1} = -\frac{4}{\phi C_c}\left\{\frac{v}{u_1} - 1 + \frac{u_2}{u_1} log\frac{v-u_2}{u_1-u_2}\right\} \tag{7}$$

where t_p is the diffusion time of particle. t_p can be expressed as

$$t_p = r_p C_c a^2 / 18m \quad , \quad C_c = 1 + 2.514(l/2a) + 0.80(l/2a)\exp\{-0.55(2a/l)\} \tag{8}$$

where l denotes the mean free path of fluid. Eqs.(7) and (8) implies that the settling length can be expressed in a non-dimensional form of particle radius a, using $t_p u_1$. Fig.6 shows the dimensionless settling length for different particle radius and density. In the figure, the least-square fitting curve is also plotted. The curve is given by

$$L^*_{set} = \frac{x_{settlingL}}{t_p u_1} = -1.108\ln(a) - 9.2052 \tag{9}$$

Obviously, the non-dimensional settling length can be expressed by a single curve.

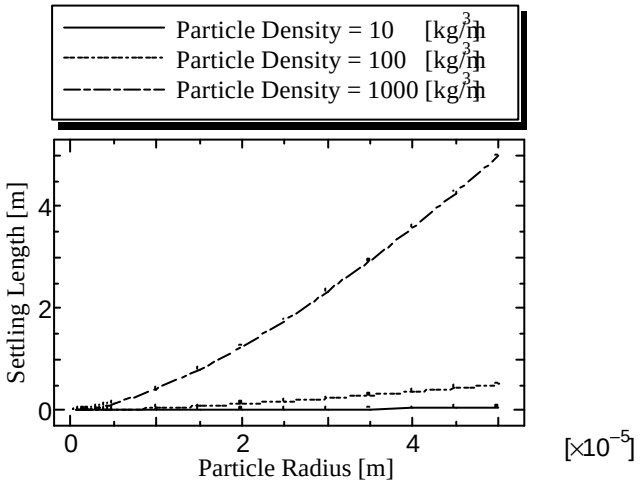

Fig.4 Settling Length for Particle Radius

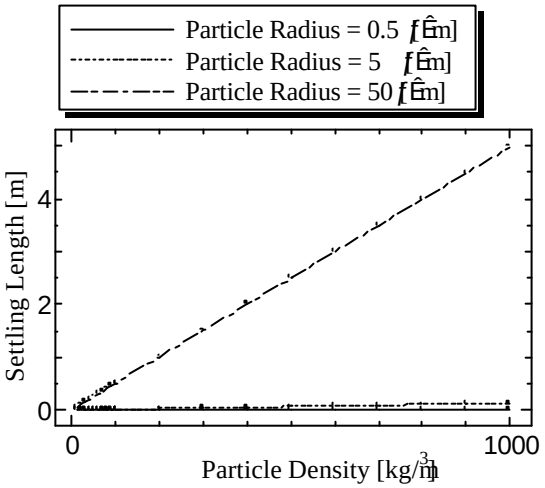

Fig.5 Settling Length for Particle Density

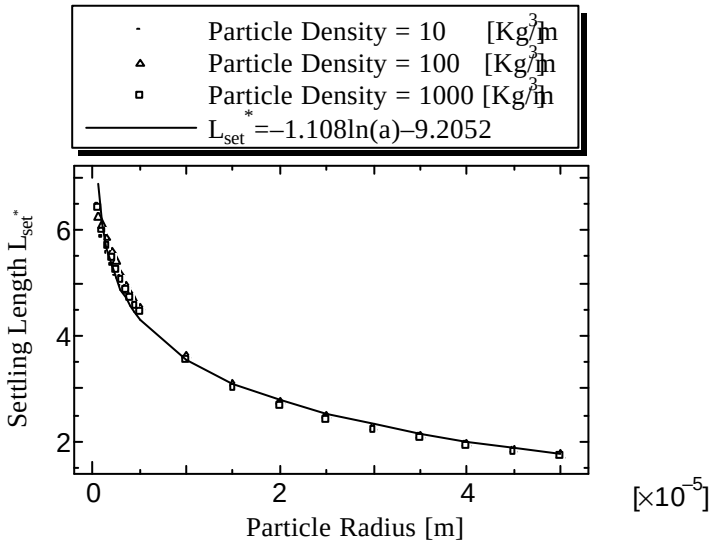

Fig.6 Non-Dimensional Settling Length and Approximation Curve

3.2 Unsteady Shock and Single Particle Case

Next, we will describe the numerical results for the case with an unsteady and a single particle. Fig.7 shows the selected results for the streamwise change of particle velocity. This is for Case B1. The upper is for the case with the shock frequency of 10[kHz], and the lower is for the case with 100[kHz]. It is clear that in the 10[kHz] case the particle passes through the shock wave only once, while in the 100[kHz] case it does several times, and experiences some accelerations and decelerations at every passing. Moreover, it is apparent that the particle motion depends on the phase angle at which the particle enters the shock wave (i.e. incidence angle). This characteristic is essentially same as in another cases.

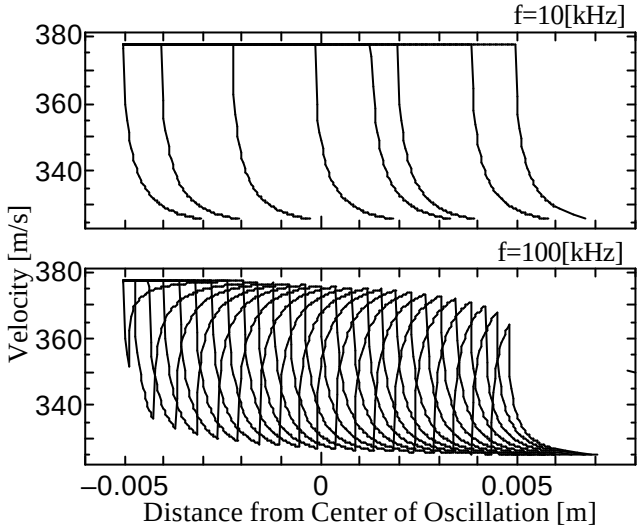

Fig.7 Streamwise Change of Particle Velocity at Different Shock Frequency (Case B1)

Fig.8 exhibits the relation between the contribution and the incidence angle. As the typical result, this figure is for Case A1 with 10[kHz]. Apparently, the drag term has the maximum and the Basset term does the minimum for the particle with the incidence angle of about 90[deg.]. This would be caused from the fact that 90[deg.] incidence corresponds to the situation where the particle and the shock move towards the downstream. And we can also see that the pressure gradient and the additional mass terms are relatively small, and the fluctuations are negligible.

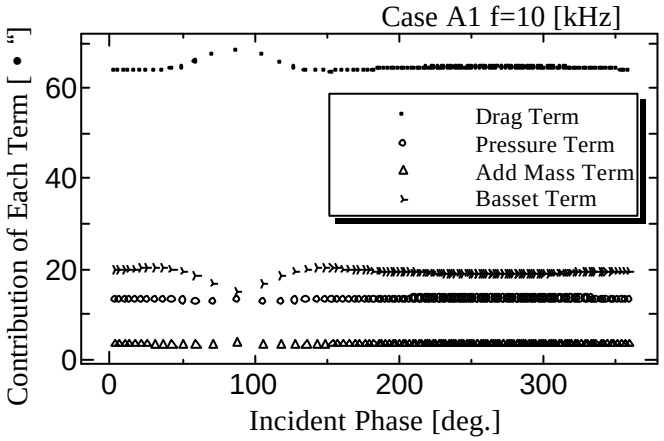

Fig.8 Relation between Contribution and Incidence Angle for Each Term

Next, let us compare the initial-phase dependence of the contributions from the drag and the Basset terms. Fig.9 and 10 show the result for the drag term and the Basset one, respectively. They are for Case A1. We can clearly find that the profiles of the 100[kHz] case are remarkably different from those of the 1 and the 10[kHz] cases. The disturbance is generated from the pass across the shock. Since the particle passes through the shock five to seven times in the 100[kHz] case, the profiles have some disturbances. Although the profiles for 1 and 10[kHz] are similar, but from the close-up view around 50[deg.] we can find some difference between the two cases. That is, around the 45[deg.] a small peak can be seen in the 10[kHz] case.

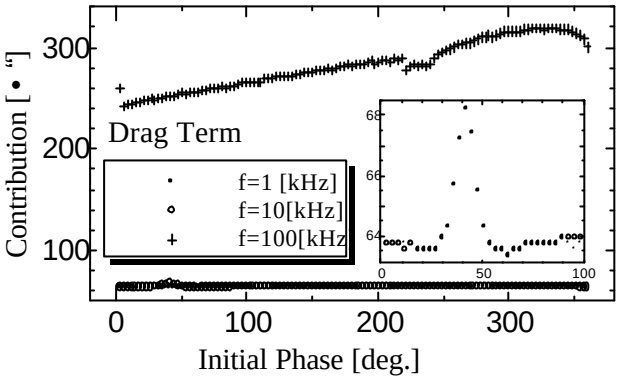

Fig.9 Comparison of Contributions for Drag Term (Case A1)

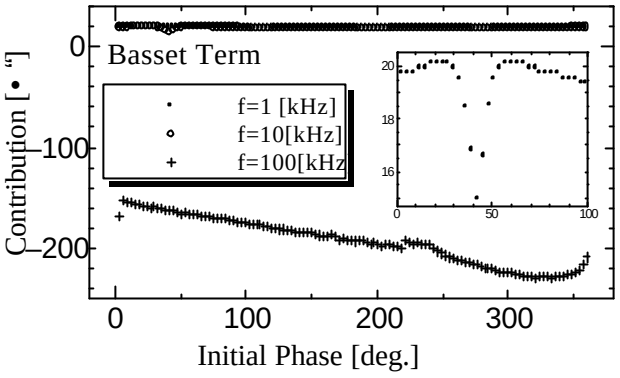

Fig.10 Comparison of Contributions for Basset Term (Case A1)

Fig.11 depicts the relation of non-dimensional settling length for the incidence angle. The shock frequency is 10[kHz]. It is clear that around the incidence angle of 90[deg.] the settling length becomes longer, and for the smaller and lighter particle the trend is more remarkable, especially in Case A1. It should be noted that for the case of 1[kHz] no influence was found.

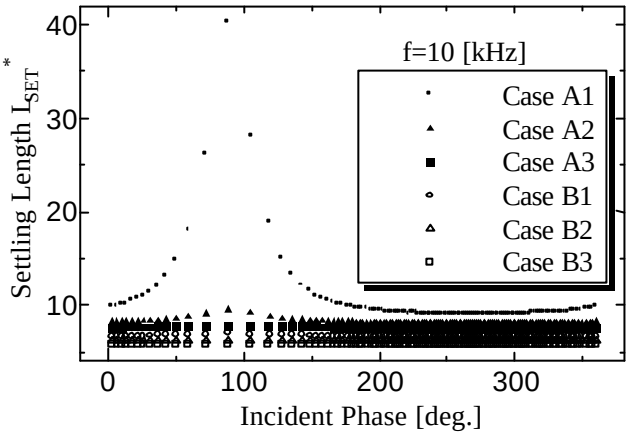

Fig.11 Relation of Non-Dimensional Settling Length for Particle Properties

3.3 Unsteady Shock and Multiple Particle Case

Finally, we will explain the cases with the particle diameter distribution. Fig.12 exhibits the expected value of particle velocity measured from the multiple particles with the diameter distribution. In the figures, lines denote the results with the diameter distribution, and symbols do those without it. Moreover, to compare the results, the steady shock case is also plotted. In the cases without the diameter distribution, we used the mean diameter for each tracer particle. From the figures, obviously, the shock oscillation and the particle diameter distribution modify the traceability of particles, especially in the case of smaller particles (i.e. MX-150). Probably, the smaller particles than the mean diameter contribute to improve the measured data. On the other hand, in the case of bigger particles (typically MX-1000), the influence is little. This would be caused from the larger inertia and the narrower distribution of such particles.

Fig.13 plots the streamwise change of estimated turbulence. The lines and symbols are same as those in Fig.12. This turbulence is generated from the shock oscillation and the particle diameter distribution (i.e. different traceability). In the cases without taking into account the particle diameter distributions, the estimated turbulence has a peak just downstream of the shock oscillation, and rapidly decays. On the contrary, in the cases with the particle diameter distribution, after having a peak, it decays gradually, and keeps a high level of 1 to 2% far downstream of the shock. The smaller particles (MX-150) have the highest peak, but the decay is the fastest, while the heavier particle (MX-1000) has the lower peak and the slow decay. It is surprising that the traceability of particle makes so large and false turbulence in spite of the fact that flow is laminar in the present study.

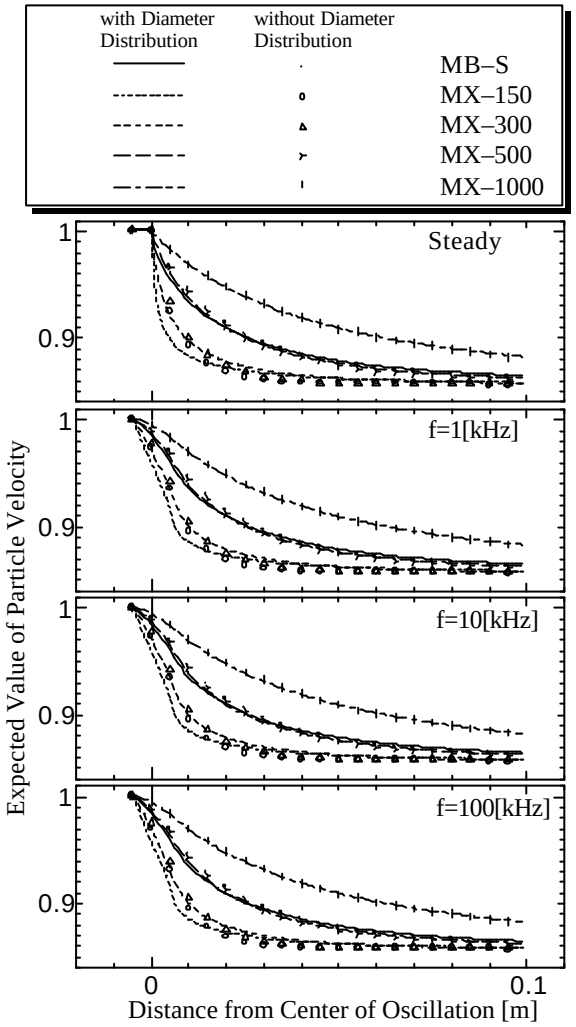

Fig.12 Streamwise Change of Expected Particle Velocity

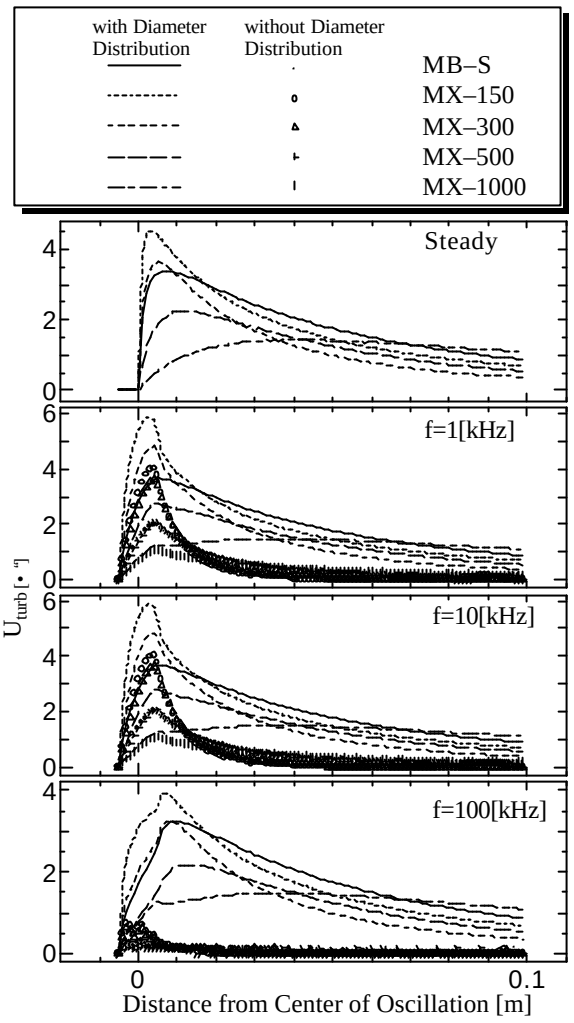

Fig.13 Streamwise Change of Estimated Turbulence

Finally, to compare the numerical results with the experimental data, we will show the experimental data in Fig.14. The experimental conditions are as follows; upstream Mach number is 1.42, total pressure is 250(kPa), total temperature is 320(K), unit Reynolds number is 2.7×10^{7} (1/m), and the data was acquired by LDV. This data was obtained in the supersonic wind tunnel in Japan Aerospace Exploration Agency (Shuto, 1997). Although the flow condition is different from that in our study, the trend is quite similar to the present computation (see Fig.13). That is, a peak is formed just downstream of the shock, turbulence decays gradually, and the peak levels are nearly same as those in our computation. From the comparison between the experiment and the present computation, we can confirm that most of the measured turbulence is caused from the bad traceability of seeding particles, and thus the turbulence data around a shock wave is so erroneous.

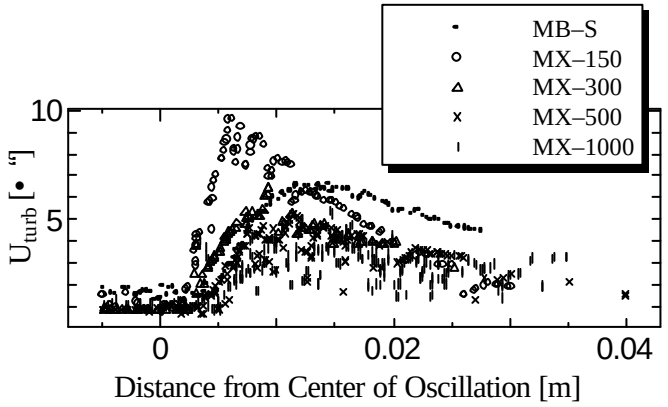

Fig.14 Experimental Data of Turbulence around Shock Wave (LDV measurement, M_1=1.42)

4. CONCLUDING REMARKS

This paper shows a numerical investigation for the motion of tracer particles in the presence of steep velocity gradient across a steady and an oscillating shock wave. Various particles with different radius and density are taken into account. The particle motions are simulated, by using Basset-Boussinesq-Oseen (BBO) equation. The distributions of physical quantities within a shock wave are obtained by the weak shock theory. Through this study, following insights have been obtained.

(1) In the case of small and light particles, the drag term is dominant, but the pressure gradient and the Basset term cannot be neglected.
(2) In the case of large density particles, only drag term is dominant.
(3) With increasing the particle diameter, the Basset term becomes smaller, and the drag term is larger. However, the contributions from the pressure gradient and the additional mass terms do not change so remarkably.
(4) As the first approximation, non-dimensional settling length can be expressed by a single curve, which is the function of a particle diameter.
(5) When a particle passes through an oscillating shock wave, the contribution from the drag and the Basset terms and settling length are modified.
(6) In the measurement around a shock wave with using tracer particles, a large measuring error would be included by the bad particle traceability.

Further studies should be performed in future, based on the present results, especially on the numerical method to detect the error quantitatively and to correct the measured data around a shock wave.

REFERENCES

Tedeschi G., Gouin H. and Elena M., Motion of Tracer Particles in Supersonic Flows. , *Experiments in Fluids*, 26, (1999), 288-296.

Thomas P. J., On the Influence of the Basset History Force on the Motion of a Particle through a Fluid., *Phys. Fluids A* 4 (9), (1992), 2090-2093.

Maurice M.S., A Method to Quantify and Correct Particle Velocity Bias in Laser Velocimetetry Measurements. , *AIAA Paper* 92-0764, (1992).

Mei R., Velocity Fidelity of Flow Tracer Particles, *Experiments in Fluids* 22, (1996), 1-13.

Dolling D.S., Bogdonoff S.M., An Experimental Investigation of the Unsteady Behavior of Blunt Fin-Induced Shock Wave Turbulent Boundary Layer Interaction. , *AIAA Paper*, 81-1287, (1981).

Dolling D.S., Or C.T., Unsteadiness of the Shock Wave Structure in Attached and Separated Compression Ramp Flow Fields. , *AIAA Paper*, 83-1715, (1983).

Coe C.F., Chyu W.J., Dods J.B., Pressure Fluctuations Underlying Attached and Separated Supersonic Turbulent Boundary Layers and Shock Waves. , *AIAA Paper*, 73-996, (1973).

Shuto H., On Traceability of Seeding Particles passing through Shock Wave, Master Thesis in Tokyo University of Science, (1997).